A Finite-Depth Wind-Wave Model. Part I: Model Description*

HANS C. GRABER

Coastal and Ocean Fluid Dynamics Laboratory, Ocean Engineering Department, Woods Hole Oceanographic Institution, Woods Hole, Massachusetts

OLE S. MADSEN

Ralph M. Parsons Laboratory, Department of Civil Engineering, Massachusetts Institute of Technology, Cambridge, Massachusetts

(Manuscript received 16 October 1987, in final form 3 February 1988)

ABSTRACT

A parametric windsea model for arbitrary water depths is presented. The model is derived from a conservation of energy flux formulation and includes shoaling, refraction, dissipation by bottom friction, as well as finite-depth modifications of the atmospheric input and nonlinear wave–wave interaction source terms. The importance of dissipation due to a rough ocean floor on the migration of the spectral peak frequency is discussed and compared with that caused by nonlinear energy transfer. Numerical simulations are used to systematically examine wave growth and the development of the spectral peak in a depth-limited ocean.

Two idealized situations of wave growth and propagation are considered to further understand the influence of bottom friction on the spectral dynamics. The first case studies the characteristics of fetch-limited wave growth in a steady, uniform wind as function of depth and bottom roughness. The second case examines the role of bottom dissipation on a fully developed deep-water spectrum propagating up a constant slope under a steady onshore blowing wind. For case 1 the growth curves and peak frequency development are plotted as a function of fetch, and wave spectra for infinite fetch and duration are shown for all depths and wave friction factors. For case 2 the evolution of total energy and peak frequency along the shelf slope are presented for stationary conditions as well as the stationary inshore energy spectra.

This numerical study reveals the following: (i) bottom friction is a finite-depth mechanism as important as the nonlinear energy transfer in controlling the spectral shape in shallow water; (ii) under the influence of bottom dissipation the positive energy transfer from wave–wave interactions to lower frequencies is reduced and causes the spectral peak to wander towards higher frequencies; (iii) equilibrium energy spectra in finite depth depend on depth and bottom roughness and occur when the nonlinear energy transfer and bottom friction source terms approximately balance each other.

1. Introduction

Surface gravity waves propagating from deep to shallow water are modified once they feel the presence of the ocean bottom. Wave–bottom interactions impose significant limitations on wave growth which depend on water depth and topographic features at the sea bed. Very few field measurements are available to understand completely the energy balance of shallow water waves and the relative importance of finite-depth processes in the evolution of the wave field. Moreover, the interaction among these depth-dependent processes and their influence on the spectral wave dynamics are not fully understood. In order to gain some insight into the dynamic and kinematic behavior of surface waves in finite-depth water, we examine the detailed space–time evolution of the wave spectrum for idealized situations in a depth-limited sea.

Recognizing the important role played by numerical wave prediction models, it is essential that these models explicitly account, as accurately as possible, for the most important physical processes. In deep water the wave energy balance is generally controlled by the interplay of energy input by the wind, nonlinear transfer of energy due to resonant wave–wave interactions, dissipation (wave breaking) and advection, while the effect of tidal and wind-driven currents generally is neglected. In shallow water, additional effects resulting from the interaction with the bottom enter the wave energy balance. Typically, depth-refraction and shoaling of waves as they propagate in water of slowly varying depth and dissipation through bottom friction will affect the evolution of the wave field. Bottom friction describes the interaction between the near-bottom wave motion and the composition of the sea bed. Through this process the waves may generate bottom bedforms (ripples)

* Woods Hole Oceanographic Institution Contribution Number: 6595.

Corresponding author address: Dr. Hans C. Graber, Coastal and Ocean Fluid Dynamics Laboratory, Ocean Engineering Department, Woods Hole Oceanographic Institution, Woods Hole, MA 02543.

and/or significant transport of sediments, which can result in considerable loss of wave energy (Grant and Madsen 1982). Other finite-depth mechanisms such as percolation, soft bottom motions and scattering off bottom irregularities (Shemdin et al. 1980) as well as tidal and wind-driven currents and mean sea level variations are important at specific locations on the continental shelf and in coastal waters, but are presently neglected in the finite-depth wave model described here.

One of the earliest studies of predicting the two-dimensional wave spectrum in shallow water (South China Sea) was described by Barnett et al. (1969) who used a general ray technique to transform waves from deep to shallow water. A source function for bottom friction based on the work of Hasselmann and Collins (1968) was also included to account for the additional dissipation felt by the surface waves. Collins (1972) studied two schemes, a parallel and irregular bottom-contour model, which incorporated attenuation by bottom friction, to assess the accuracy of shallow water sea state predictions. Hasselmann et al. (1973) investigated the mechanism responsible for the observed swell decay during JONSWAP. They assumed that tidal currents were dominating wave-induced velocities in the near-bottom boundary layer. This assumption appears to contradict results obtained by Grant and Madsen (1979). A routinely operated wave forecasting model for the continental shelf areas around England which considered only depth-refraction and shoaling was discussed by Golding (1978). In an updated version (Golding 1983) a dissipative bottom friction term (Collins 1972) with a constant friction factor was added. Cavaleri and Rizzoli (1978) have described a characteristic ray model of the Adriatic Sea which also incorporated these finite-depth effects. The hybrid wave model GONO, operationally run for the North Sea, models bottom friction with the JONSWAP form but disregards depth-refraction effects (Janssen et al. 1984). The HYPAS wave prediction model developed by Günther and Rosenthal (1983a, 1983b) neglects bottom friction in the parametric windsea description but bottom dissipation is introduced in the decoupled propagation of swell components. Janssen and de Voogt (1985) investigated the effect of a linearized JONSWAP bottom friction term on a windsea described by the Kruseman spectrum. More recently the SWIM (1985) study intercompared three operational shallow water wave models for two idealized wave generation cases and for a severe North Sea storm. The objective of this study was to understand and improve the representation of finite-depth wave mechanisms in numerical models.

In this paper we present a finite-depth parametric windsea model developed by Graber (1984) and verified in a complex North Atlantic frontal system by Graber and Madsen (1985). The deep-water HYPA model developed by Hasselmann et al. (1976) and Günther et al. (1979) is rederived based on the concept of energy flux. The choice of energy flux to represent the directional relaxation of a wind-driven wave field is an alternative method to that of Günther et al. (1981) who used wave momentum considerations to incorporate the response of the windsea to changes in the wind direction. Similarly, Donelan (1977) developed a simple, parametric wave model using a wave momentum formulation which was later revised by Schwab et al. (1984). Applications of the Donelan model have been limited to deep-water waves only. The present model includes finite-depth effects and is tested for idealized situations of fetch-limited wave growth over horizontal and gently sloping bottoms with bottom friction representative of a range of bottom sediments. These numerical simulations are used to further understand the influence of bottom friction on the evolution of the spectrum in depth-limited generation cases.

2. Governing equations for windsea model: Physical space

The surface wave field is generally described by the two-dimensional wave spectrum $\Psi(\mathbf{k})$ in wave number space or by $F(f, \theta)$ as a function of frequency f and direction θ. The inclusion of a mean wave direction as one of the parameters describing the windsea is conveniently carried out by adopting a vector quantity which we have chosen as the wave energy flux

$$\mathcal{F}(\mathbf{k}, \mathbf{r}, t) = \mathbf{c}_g(\mathbf{k}, \mathbf{r})\Psi(\mathbf{k}, \mathbf{r}, t) \tag{1}$$

where $\mathbf{k} = (k_x, k_y)$ and $\mathbf{r} = (x, y)$ are the wavenumber and position vectors, respectively, t is time, and $\mathbf{c}_g$ is the group velocity vector.

The transport equation for the surface wave field in a plane ocean with variable bottom topography was originally given by Hasselmann (1960),

$$\frac{D\Psi}{Dt} = \frac{\partial \Psi}{\partial t} + (\dot{\mathbf{r}} \cdot \nabla_r)\Psi + (\dot{\mathbf{k}} \cdot \nabla_k)\Psi = T \tag{2}$$

where

$$\dot{\mathbf{r}} \equiv \nabla_k \omega(\mathbf{k}, \mathbf{r}) = \mathbf{c}_g(\mathbf{k}, \mathbf{r}) \tag{3}$$

$$\dot{\mathbf{k}} \equiv -\nabla_r \omega(\mathbf{k}, \mathbf{r}) \tag{4}$$

are the ray equations for a steady, inhomogeneous medium as defined by the dispersion relation $\omega^2 = (2\pi f)^2 = gk \tanh kh$, in which $k \equiv |\mathbf{k}|$ and $h = h(\mathbf{r})$ is the local water depth. The T describes all processes generating or dissipating energy of the wave field at each wave component. Here D/Dt describes the Lagrangian rate of change relative to the advection of a wave group along the ray paths as determined by (3) and (4).

A conservation equation for wave energy flux can be derived from the following identity

$$\frac{D\mathcal{F}}{Dt} \equiv \frac{\partial \mathcal{F}}{\partial t} + (\dot{\mathbf{r}} \cdot \nabla_r)\mathcal{F} + (\dot{\mathbf{k}} \cdot \nabla_k)\mathcal{F}$$

$$= \mathbf{c}_g \frac{D\Psi}{Dt} + \Psi \frac{D\mathbf{c}_g}{Dt}. \quad (5)$$

The net rate of change of energy flux can be represented by a sum of four mechanisms

$$\mathbf{c}_g \frac{D\Psi}{Dt} = \mathcal{T}(\mathbf{k})$$

$$= \mathcal{T}_{in}(\mathbf{k}) + \mathcal{T}_{nl}(\mathbf{k}) + \mathcal{T}_{dis}(\mathbf{k}) + \mathcal{T}_{bf}(\mathbf{k}). \quad (6)$$

From (2) it follows that $\mathcal{T} = \mathbf{c}_g T$, the net source function for the wave number energy flux, includes processes represented by atmospheric input by the wind $\mathcal{T}_{in}$, nonlinear transfer of energy among resonantly interacting wave modes $\mathcal{T}_{nl}$, dissipation by wave breaking $\mathcal{T}_{dis}$, and attenuation due to bottom friction $\mathcal{T}_{bf}$. The additional term on the right-hand-side of (5) is the differential flux of wave energy due to the rate of change of the group velocity along a ray (Note: This term vanishes in an ocean of constant depth).

A more convenient form of the transport equation is obtained in frequency–direction space (for details see Graber 1984),

$$\frac{\partial \mathcal{E}}{\partial t} + (\dot{\mathbf{r}} \cdot \nabla_r)\mathcal{E} + (\dot{\mathbf{k}} \cdot \nabla_k \theta)\frac{\partial \mathcal{E}}{\partial \theta} = \mathcal{S} + \mathcal{E}(\nabla_r \cdot \mathbf{c}_g)$$

$$+ E(\dot{\mathbf{k}} \cdot \nabla_k \theta)\frac{\partial \mathbf{c}_g}{\partial \theta} - \frac{\mathcal{E}}{\mathcal{J}}(\mathbf{c}_g \cdot \nabla_r)\mathcal{J} \quad (7)$$

by substituting $\mathcal{J} \cdot \mathcal{E}(f, \theta)$ for $\mathcal{F}(\mathbf{k})$ in (5). The Jacobian $\mathcal{J}$ is defined by

$$\mathcal{J} \equiv \partial(f, \theta)/\partial(k_x, k_y) = \frac{cc_g}{2\pi\omega} \quad (8)$$

with $c = (g/\omega)\tanh kh$ the phase velocity, $\mathcal{S} = \mathcal{J}^{-1}\mathcal{T} = \mathcal{S}_{in} + \mathcal{S}_{nl} + \mathcal{S}_{dis} + \mathcal{S}_{bf}$ and the energy flux density is given by the product of depth-dependent group velocity and wave spectrum, i.e.,

$$\mathcal{E}(f, \theta, h) = \mathbf{c}_g(f, h)E(f, \theta, h). \quad (9)$$

A consistent approach on the self-similarity of depth-dependent frequency spectra was originally demonstrated by Kitaigorodskii et al. (1975) and experimental evidence was provided by Bouws et al. (1985). Thus we chose the TMA spectral shape

$$E(f, \theta, h) = \Phi(\omega_h)E_J(f)\frac{2}{\pi}\cos^2(\theta - \theta_0) \quad (10)$$

where the depth transformation factor is defined as

$$\Phi(\omega_h) = \chi^{-2}[1 + \omega_h^2(\chi^2 - 1)]^{-1} \quad (11)$$

with χ the solution to the transcendental equation $\chi \tanh(\omega_h^2 \chi) = 1$ and $\omega_h = 2\pi f(h/g)^{1/2}$.

The one-dimensional windsea spectrum, $E_J(f)$, is described by the JONSWAP spectral shape (Hasselmann et al. 1973) which is determined from the set of five free parameters $a_i = [f_m, \alpha, \gamma, \sigma_a, \sigma_b]$,

$$E_J(f; a_i) = E_{PM}(f; a_i)\gamma^{\exp[-(f/f_m - 1)^2/2\sigma^2]} \quad (12)$$

with

$$E_{PM}(f; a_i) = \alpha g^2(2\pi)^{-4} f^{-5} \exp\left[-\frac{5}{4}\left(\frac{f}{f_m}\right)^{-4}\right] \quad (13)$$

the Pierson and Moskowitz (1964) spectrum referring to a fully developed sea.

The cosine-squared angular spreading function for $\pm\pi/2$ about the mean windsea direction, θ_0, independent of frequency is adopted here in (10) to apply for any depth. It should be recognized that this choice of spreading function represents a simplification of the directional characteristics of waves in variable water depth. Thus, depth-refraction would potentially focus the wave energy in a smaller directional interval around the mean direction as well as produce an asymmetric distribution around the mean. To account for these effects would require at least two additional parameters to be included. There are, however, insufficient observational data to develop an angular spreading function which accounts for these effects. Consequently we have adopted the simple cosine-squared spreading function which has been used extensively in deep-water wind-wave models.

The mean windsea direction, θ_0, introduces a sixth spectral parameter which can be determined in an analogous way to that suggested by Günther et al. (1981) from the x (East) and y (North) components of the total energy flux I,

$$I_x = \int_0^{2\pi}\int_0^{\infty} |\mathcal{E}| \sin\theta df d\theta \quad (14)$$

$$I_y = \int_0^{2\pi}\int_0^{\infty} |\mathcal{E}| \cos\theta df d\theta \quad (15)$$

from which it follows

$$\theta_0 = \tan^{-1}\left[\frac{I_x}{I_y}\right] \quad (16)$$

(A positive clockwise convention from north is assumed.)

3. Governing equations for windsea model: Parametric space

The concept of a parametric windsea description has originally been proposed by Hasselmann et al. (1973, 1976) and was further developed and extensively tested in deep water by Günther et al. (1979, 1981). In order to translate the transport equation for energy flux (7) into a set of partial differential equations for the parameters a_i, we need to construct appropriate mapping functionals which reveal the JONSWAP parameters.

Following the approach in Günther et al. (1981) we find

$$a_i = \phi_i\{\mathcal{E}\} = \varphi_i\left\{\frac{\int [\mathcal{E}_x^2(f,\theta,h) + \mathcal{E}_y^2(f,\theta,h)]^{1/2} d\theta}{c_g(f,h)\Phi(\omega_h)}\right\} = \varphi_i\{E(f)\} \quad (17)$$

where $a_1 = f_m$, $a_2 = \alpha$, $a_3 = \gamma$, $a_4 = \sigma_a$, $a_5 = \sigma_b$. With this definition the resulting mapping operators ϕ_i' are identical to φ_i', which were previously defined by Günther et al. (1979). For the directional parameter $a_6 = \theta_0$ the mapping operation is carried out directly on the energy flux vector (Graber and Madsen 1982). Making use of the definition of θ_0 in (16), ϕ_6 can be stated as

$$a_6 = \phi_6\{\mathcal{E}\} = \tan^{-1}\left\{\frac{\int\int \mathcal{E}_x d f d\theta}{\int\int \mathcal{E}_y d f d\theta}\right\}. \quad (18)$$

The functional or Fréchet derivative determined from (18) is

$$\phi_6'\{\delta\mathcal{E}\} = \frac{3\pi}{8}\frac{\int\int (\cos\theta_0 \delta\mathcal{E}_y - \sin\theta_0 \delta\mathcal{E}_x) df d\theta}{\int\int \mathcal{E}\, df d\theta}. \quad (19)$$

Details on the derivation of (19) may be found in Graber (1984).

Applying the mapping functionals ϕ_i' to the conservation equation of energy flux one arrives at six, coupled transport equation for the windsea parameters a_i

$$\frac{\partial a_i}{\partial t} + D_{ijx}\frac{\partial a_j}{\partial x} + D_{ijy}\frac{\partial a_j}{\partial y} = S_i + R_i \quad \text{for } i,j = 1,\cdots,6 \quad (20)$$

in which the components of the depth-dependent propagation matrix D_{ij} are

$$D_{ijx} = \phi_i'\left\{c_{gx}\frac{\partial \mathcal{E}}{\partial a_j}\right\}, \quad D_{ijy} = \phi_i'\left\{c_{gy}\frac{\partial \mathcal{E}}{\partial a_j}\right\} \quad (21)$$

with $c_{gx} = |\mathbf{c}_g| \sin\theta$, $c_{gy} = |\mathbf{c}_g| \cos\theta$,

$$S_i = \phi_i'\{\mathcal{S}_{in} + \mathcal{S}_{nl} + \mathcal{S}_{dis} + \mathcal{S}_{bf}\} \quad (22)$$

and

$$R_i = \phi_i'\left\{\mathcal{E}(\nabla_r \cdot \mathbf{c}_g) + \mathbf{c}_g(\dot{\mathbf{k}}\cdot\nabla_k\theta)\frac{\partial E}{\partial\theta} - \frac{\mathcal{E}}{\mathcal{A}}(\mathbf{c}_g\cdot\nabla_r)\mathcal{A} - \frac{\partial \mathcal{E}}{\partial h}(\mathbf{c}_g\cdot\nabla_r h)\right\}. \quad (23)$$

The source functions S_i are modified to reproduce a rapidly approaching quasi-equilibrium (Günther and Rosenthal 1983a). The additional terms enumerated in R_i result from mapping the refraction and group velocity divergence terms onto the parameter space. The last term in R_i results from a variation $\delta\mathcal{E}$ in $\mathcal{E}$ due to a change δh in the water depth h, i.e.,

$$\delta\mathcal{E} = \frac{\partial \mathcal{E}}{\partial a_j}\delta a_j + \frac{\partial \mathcal{E}}{\partial h}\delta h.$$

Details on the derivation of the parametric form of R_i is given in appendix A. The expressions for D_{ij} are given in Table 1. The terms D_{4j}, D_{5j}, D_{i4}, and D_{i5} for $i,j = 1,\cdots,6$, have been omitted since their contribution to the overall transport equation is small. As a matter of fact the parameters σ_a and σ_b are determined from analytic expressions involving γ only (Günther et al. 1979).

TABLE 1. The depth dependent coefficients D_{ij} (The ξ_i and J_i are given in appendix B).

	j			
i	1	2	3	6
1	$c_{gm}(1 + 5\xi_0)$	$-c_{gm}\frac{f_m}{\alpha}\xi_0$	$-c_{gm}\frac{f_m}{\gamma}\xi_0$	$-c_{gm}f_m\xi_0$
2	$c_{gm}\frac{\alpha}{f_m}(\xi_1 + 3.61\xi_0)$	$c_{gm}(\xi_2 - 0.722\xi_0)$	$-c_{gm}\frac{\alpha}{\gamma}0.722\xi_1$	$c_{gm}\alpha(\xi_2 - 0.722\xi_0)$
3	$c_{gm}\frac{\gamma}{f_m}(21.39\xi_0 - \xi_1)$	$c_{gm}\frac{\gamma}{\alpha}(1 - \xi_1 - 4.28\xi_0)$	$c_{gm}(1 - 4.28\xi_0)$	$c_{gm}\gamma(1 - \xi_1 - 4.28\xi_0)$
6	$-\frac{9}{64}gf_m^{-2}\frac{J_3}{J_2}$	$\frac{3}{128}g(\alpha f_m)^{-1}\frac{J_3}{J_2}$	$\frac{3}{128}gf_m^{-1}\frac{J_3}{J_2}$	$\frac{3}{64}gf_m^{-1}\frac{J_3}{J_2}$

4. Source functions and directional relaxation

The growth and decay of surface waves is the result of various linear and nonlinear physical processes transferring energy to and from the wave field as well as redistributing energy within the spectrum itself. The following source functions are considered to influence significantly the evolution of the spectral shape in an ocean of finite depth.

a. Atmospheric input by the wind

Wave generation takes place in several phases. In the linear phase wave growth is due to random pressure fluctuations of a turbulent wind over a calm ocean surface (Phillips 1957). This mechanism is effective only in the initial stages of wave growth. Subsequently the influx of energy from the wind is continued by an instability mechanism coupling the wave field and the mean boundary layer flow (Miles 1957), leading to an exponential growth in energy density. The Miles mechanism is generally represented by the parameterization based on the results of Snyder et al. (1981),

$$T_{in}(f, \theta, h) = \beta(f, \theta, h)E(f, \theta, h) \qquad (24)$$

where the growth function is given by

$$\beta(f, \theta, h) = \begin{cases} B\dfrac{\rho_a}{\rho_w}\omega\left[\dfrac{U_{10}\cos(\theta - \Theta)}{c} - 1\right], & \left|\dfrac{U_{||}}{c}\right| > 1 \\ 0, & \left|\dfrac{U_{||}}{c}\right| \leqslant 1. \end{cases}$$

This functional form was deduced from direct measurements of the work done by the wave-induced air pressure fluctuations over the sea surface. Here ρ_a and ρ_w refer to the densities of air and water, $\omega = 2\pi f$, c is the depth-dependent phase velocity, θ and Θ are the wave component and mean wind direction, respectively. Thus, $U_{10}\cos(\theta - \Theta) \equiv U_{||}$ is the wind speed at 10 m parallel to the wave direction θ. The coefficient B was determined by Snyder et al. (1981) to vary from 0.2 to 0.3.

The minimal input case discussed by Hasselmann et al. (1976) is adopted here which means that dissipation is assumed to be zero in the frequency range $f < 2f_m$. Hence, we consider only the net input of the atmosphere, i.e., $\mathcal{S}_{net} = \mathcal{S}_{in} + \mathcal{S}_{dis}$. Since wave growth depends only on the ratio of the wind speed to phase velocity, applying the operator ϕ_i' to $\mathcal{S}_{net}$ yields a modified input source function for finite depth, i.e.,

$$\begin{aligned} S^1_{net} &= S^1_{in} + S^1_{dis} \approx 0 \\ S^2_{net} &= S^2_{in} + S^2_{dis} = \alpha f_m Q(\nu_h) = \alpha f_m Q(\kappa) \\ S^3_{net} &= S^3_{in} + S^3_{dis} \approx 0 \end{aligned} \qquad (25)$$

where $\nu_h = f_m U_{||}\chi(\omega_h)/g$ and $\kappa = k_m U_{||}^2/g$ with $k_m = k(f_m)$ denoting the wave number corresponding the peak frequency. For the function $Q(\nu_h)$ we chose the same expression as derived from the fetch-limited behavior f_m and α (Günther et al. 1979), namely

$$S^2_{net} = 0.005022\alpha f_m \nu_h^{4/3} = 0.000433\alpha f_m \kappa^{2/3}. \qquad (26)$$

Note, in the deep-water limit, (26) reduces exactly to the expression given by Günther et al. (1979, 1981). As found by Hasselmann et al. (1976) the atmospheric input terms for f_m and γ parameters (S^1_{net} and S^3_{net}) are negligibly small and therefore omitted.

The heuristic lower limit of the windsea peak frequency is generally accepted as the frequency of a fully-developed sea (Pierson and Moskowitz 1964). At the Pierson–Moskowitz frequency, f_{PM}, the parameter $U_{||}/c = 0.82$ in deep water and adopting this concept also for fully developed sea states in finite depth leads to

$$f_{PM} = \frac{0.13g\tanh k_{PM}h}{U_{10}\cos(\theta_0 - \Theta)}. \qquad (27)$$

In the deep-water limit this expression reduces to the original Pierson–Moskowitz relation. In the shallow water limit, for which

$$c_{max}(f_{PM}) = (gh)^{1/2} \qquad (28)$$

it would not be possible to reach fully developed conditions if $U_{||} > 0.82(gh)^{1/2}$. This result is supported by the results of Bouws et al. (1987) who concluded from their analysis of depth-dependent wave spectra that choosing $U_{||}/c$ as the regression variable did not yield a depth-independent quasi-equilibrium line. Alternatively, (27) can be expressed in terms of a non-dimensional wave number as defined by Bouws et al. (1985)

$$\kappa = \frac{k(f_{PM})U_{||}^2}{g} = 0.6672. \qquad (29)$$

In shallow water, wave growth is ultimately limited by dissipation associated with wave breaking. McCowan's (1894) result for a limiting wave height to water depth ratio, $H/h = 0.78$, is often adopted as a shallow water breaking criterion. Presently, this limiting process is not explicitly included in our model since the inclusion of a realistic representation of the dissipation due to bottom friction has shown that a quasi-equilibrium state is attained before the shallow-water breaking limit is approached.

b. Nonlinear transfer by resonant wave–wave interactions

The general form of the "exact" nonlinear transfer terms T_{nl} is given by the Boltzmann integral expressing the rate of change of energy of the wave spectrum $\Psi(\mathbf{k})$ at wavenumber $\mathbf{k}_4$ due to nonlinear wave–wave interactions (Hasselmann and Hasselmann 1985),

$$T_{nl}(\mathbf{k}_4) = \int \sigma\omega_4\delta(\mathbf{k}_1 + \mathbf{k}_2 - \mathbf{k}_3 - \mathbf{k}_4) \times \delta(\omega_1 + \omega_2 - \omega_3 - \omega_4)[N_1N_2(N_3 + N_4) - N_3N_4(N_1 + N_2)]d\mathbf{k}_1 d\mathbf{k}_2 d\mathbf{k}_3 \quad (30)$$

where $N_i \equiv N(\mathbf{k}_i) = \Psi(\mathbf{k}_i)/\omega_i$ stands for wave action densities, $\omega_i = (gk_i \tanh k_i h)^{1/2}$ are the wave frequencies corresponding to the ith wavenumber, and σ represents a complex scattering coefficient describing the coupling strength of four-way resonantly interacting wave modes. Hasselmann et al. (1973) deduced that the general form of the nonlinear transfer scales as

$$T_{nl}(f, \theta) = \alpha^3 g^2 f_m^{-4} \psi(f/f_m, \theta) \quad (31)$$

where ψ is a dimensionless function describing the spectral shape. Based on similarity arguments, Herterich and Hasselmann (1980) have calculated the finite-depth interaction for a narrow-band wave spectrum. It was concluded from their analysis that the finite-depth source function of the one-dimensional nonlinear transfer can be scaled by a depth-dependent factor R, i.e.,

$$S_{nl}(f, h) = R(\omega_{hm})S_{nl}(f, \infty) \quad \text{for} \quad \omega_{hm} \geq 0.7. \quad (32)$$

Confirmation of relation (32) and the validity of shape similarity for directional distributions was made by Hasselmann and Hasselmann (1981) who computed the interaction rates for a representative set of spectra $F(f, \theta, h)$ from the "exact" nonlinear transfer integral (30). Examination of the results of Hasselmann and Hasselmann leads to an expression for the proportionality factor

$$R = R(\omega_{hm}) = \frac{\chi^4}{[1 + \omega_{hm}^2(\chi^2 - 1)]^2}. \quad (33)$$

Furthermore, it is found from their results that relation (32) with R given by (33) is valid for values of $\omega_{hm} \geq 0.4$. For smaller values of ω_{hm} the nonlinear transfer exceeds the deep-water values by more than one order of magnitude. For this region the weakly nonlinear interaction theory is expected to break down. Additional details on the computations and parameterizations of the nonlinear transfer is given in Hasselmann and Hasselmann (1985).

Therefore, we treat the nonlinear source function S_{nl} in the same manner as Günther et al. (1979, 1981). Extension to the finite-depth case is obtained by multiplying the deep-water values with the scaling factor R. In summary, we arrive at the following parametric expressions for S_{nl}:

$$S_{nl}^1 = -0.2548\alpha^2 f_m^2(\gamma - 1)R(\omega_{hm}) \quad \text{for} \quad \gamma \geq 1$$

$$S_{nl}^2 = -5\alpha^3 f_m R(\omega_{hm})$$

$$S_{nl}^3 = -16(\gamma - \gamma_0)\alpha^2 f_m R(\omega_{hm})$$

$$S_{nl}^4 = -[25.5\sigma_a - 0.5\sigma_b - 1.74p]\alpha^2 f_m R(\omega_{hm})$$

$$S_{nl}^5 = -[25.5\sigma_b - 0.5\sigma_a - 2.26p]\alpha^2 f_m R(\omega_{hm}) \quad (34)$$

where

$$\gamma_0 = \begin{cases} 3.3, & \kappa > 1.011 \\ 1 + 3.905(\kappa - 0.6672)^{1/2}, & 0.6672 \leq \kappa \leq 1.011 \\ 1, & \kappa < 0.6672 \end{cases}$$

$$p = 16/(\gamma + 0.7)^2.$$

c. Dissipation by bottom friction

In shallow water the interaction of the wave-induced near-bottom flow with the microtopography of the sea bottom develops a boundary layer as a result of a non-vanishing boundary shear stress. Within this boundary layer mechanical energy is lost through viscous effects and hence attenuates the surface waves. Kajiura (1968) derived a simple expression of the average rate of dissipation of energy due to bottom friction for stationary waves. In a rigorous theoretical treatment, Hasselmann and Collins (1968) derived a general expression for the dissipation rate of a wave spectrum. Both analyses were based on a quadratic friction law,

$$\tau_b = \frac{1}{2}\rho f_w \mathbf{u}_b |\mathbf{u}_b| \quad (35)$$

where τ_b is the shear stress at the sea bottom, $\mathbf{u}_b$ is the near-bottom wave velocity just outside the wave boundary layer, and f_w is the wave friction factor. Considerable interest has been given to develop expressions for the wave friction factor, since the initial work of Jonsson (1966). Theoretical expressions for f_w were obtained by Kajiura (1964, 1968) and Grant (1977) introducing the concept of an eddy viscosity to close the dynamical equations. Trowbridge and Madsen (1984) improved on the formulation of f_w by including more realistic eddy viscosity models. In general the wave friction factor is found to be a slowly varying function of the parameters characterizing the flow and the bottom roughness. A more detailed treatment of this subject can be found in Grant and Madsen (1986).

Recently, Grant and Madsen (1982) argued that the fluid–sediment interaction must be accounted for as precisely as possible for accurate predictions of wave energy loss due to bottom friction. From analyses of laboratory data they developed a formula for the equivalent bottom roughness of a moveable bed under the action of waves. Their roughness, which depends on sediment and near-bottom wave characteristics, may in turn be used in conjunction with their model, Grant and Madsen (1986), to predict friction factors for a moveable bed in the presence of waves. Figure 1 presents the wave friction factors, f_w, as a function of the near-bottom wave orbital excursion amplitude, A_b,

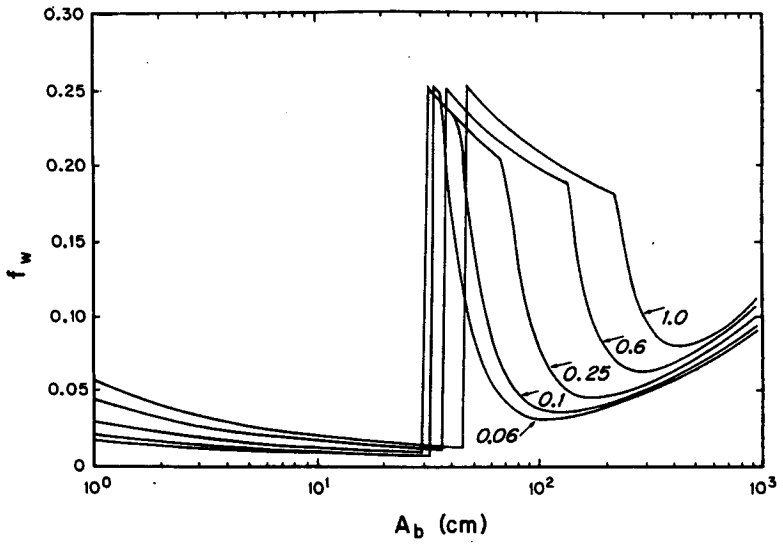

FIG. 1. Movable bed friction factor, f_w vs near-bottom orbital excursion amplitude, A_b, obtained from Grant and Madsen (1982) for a 10 s wave as a function of diameter (mm) of a quartz sand.

for various diameter quartz sands predicted by the Grant-Madsen (1982) model. Although the predicted values of f_w depend on wave period, this dependency is sufficiently weak to regard the results presented in Fig. 1 for a period of 10 s to be representative for the range of periods expected in the marine environment.

Physically the friction factor variation shown in Fig. 1 represents for low values of A_b the flow resistance of a flat, immobile bed, i.e., with a roughness equal to the sediment diameter. As A_b increases the wave–sediment interaction reaches a threshold value (Madsen and Grant 1976) at which sediment starts to move. Once the threshold value is exceeded the sediment–fluid interface deforms and wave-generated ripples appear. The bottom roughness now scales with the ripple geometry, which results in a dramatic increase in friction factors. Further increase of the flow intensity, i.e., A_b, "smoothes" the ripples, first gradually then rapidly, and results in corresponding rates of decrease of the friction factor with increasing A_b until the ripples are practically washed out and the bed is returned to its initial flat state. However, in contrast to the immobile, flat bed state, sediment is now moving back and forth above the bed. Associated with the sediment in motion is an apparent increase in roughness reflected by the friction factor, for large A_b values, reaching a minimum value which is larger than the value associated with the initial flat bed. Beyond this minimum of the friction factor for a mobile flat bed its variation is controlled by the increase in intensity of sediment movement above the bed.

The spectral dissipation function due to bottom friction can be approximated according to Collins (1972) and Madsen et al. (1988) by

$$T_{bf} = \frac{1}{2} f_w \frac{\omega^2}{g \sinh^2 kh} \langle u_b \rangle E(f, \theta, h) \tag{36}$$

where the rms bottom velocity

$$\langle u_b \rangle = u_{br} = \left(2 \int_0^{2\pi} \int_0^{\infty} \frac{\omega^2}{\sinh^2 kh} E(f, \theta, h) df d\theta \right)^{1/2} \tag{37}$$

is representative of the near-bottom velocity field. The resulting parametric source functions for the bottom friction term can be derived from applying the mapping functionals ϕ_i' to (36). The final expressions for parameters f_m, α and γ are

$$S_{bf}^1 = (2\pi)^2 f_w \frac{f_m^3}{g} K\Gamma u_{br}$$

$$S_{bf}^2 = -(2\pi)^2 f_w \alpha \frac{f_m^2}{g} u_{br}[I_2 + 0.722 K\Gamma]$$

$$S_{bf}^3 = -(2\pi)^2 f_w \gamma \frac{f_m^2}{g} u_{br}[(\chi^2 - 1) - I_2 + 4.28 K\Gamma] \tag{38}$$

where the representative bottom velocity is computed from

$$u_{br} = \frac{\alpha^{1/2} g}{(2)^{1/2} \pi} f_m^{-1} I_1^{1/2} \tag{39}$$

and the integrals I_1 and I_2 must be evaluated numerically

$$I_1 = \omega_{hm} \int_0^\infty \omega_h^{-3} \frac{(\chi^2 - 1)}{\chi^2[1 + \omega_h^2(\chi^2 - 1)]} \times \psi\left(\frac{\omega_h}{\omega_{hm}}, \gamma, \sigma\right) d\omega_h \quad (40)$$

$$I_2 = \omega_{hm}^{-3} \int_{1.35\omega_{hm}}^{2.0\omega_{hm}} \omega_h^2(\chi^2 - 1) d\omega_h. \quad (41)$$

The shape function ψ is defined as

$$\psi\left(\frac{\omega_h}{\omega_{hm}}, \gamma, \sigma\right) = \exp\left\{-\frac{5}{4}\left(\frac{\omega_h}{\omega_{hm}}\right)^{-4} + \ln\gamma \exp\left[-\left(\frac{\omega_h}{\omega_{hm}} - 1\right)^2 \Big/ 2\sigma^2\right]\right\}$$

and the functions K and Γ are expressed as

$$K = \left(\frac{\sigma^2}{20\sigma^2 + \ln\gamma}\right), \quad \sigma = \frac{1}{2}(\sigma_a + \sigma_b) \quad (42)$$

$$\Gamma = (\chi^2 - 1)\left[\frac{1 - \omega_{hm}^2(\chi^2 + 1)}{1 + \omega_{hm}^2(\chi^2 - 1)}\right]. \quad (43)$$

d. Directional relaxation of a windsea

When waves propagate into a region where the local direction of the wind differs from the direction of the waves, the wind component perpendicular to the wave trajectory will attempt to turn the waves so that they eventually become aligned with the direction of the wind. Hasselmann et al. (1980) and Günther et al. (1981) have shown that the high-frequency components of the spectrum almost instantaneously respond to a sudden change in the wind direction. The nonlinear interactions are thought of to be the mechanism which translates changes in the energy flux direction of the high-frequency tail to lower frequencies, thus resulting in a turning of the entire spectrum towards the new wind direction. In open water the mean wave direction would eventually become parallel to the new wind direction, while this, as shown by Donelan (1980), would not necessarily be the case for fetch-limited situations.

For parametric wave models a reasonable choice, expressing this directional response, is the mean direction averaged over the windsea spectrum as given by (16). The prognostic equation for the parameter $a_6 = \theta_0$ reads then

$$\frac{\partial a_6}{\partial t} + \sum_{j=1}^{6}\left(D_{6jx}\frac{\partial a_j}{\partial x} + D_{6jy}\frac{\partial a_j}{\partial y}\right) = S_6 + R_6. \quad (44)$$

The functional form of S_6 can directly be deduced from applying the operator ϕ_6' to the Snyder et al. (1981) type input term (24). From this it follows that

$$S_6 = -\frac{3\pi^3}{8}\frac{\rho_a}{\rho_w} B \frac{I_3}{I_4}\frac{f_m^2}{g} U_{10} \sin(\theta - \theta_0) \quad (45)$$

where the integrals I_3 and I_4 are given by $\int \mathcal{E}/c_g df$ and $\int \mathcal{E}\, df$, respectively. The nondimensional form of these integrals are shape functions proportional to $(f/f_m)^{-4}$ and $(f/f_m)^{-6}$, respectively. For the momentum approach of Günther et al. (1981), the identical expression of S_6 can be determined except with I_3 and I_4 now expressed in terms of wave momentum and proportional to $(f/f_m)^{-2}$ and $(f/f_m)^{-4}$, respectively.

For deep-water conditions, Günther et al. (1981) determined from data the value of the proportionality constant $r = 0.21 \times 10^{-2}$ radians. It is reassuring to note that the deep-water value obtained from (45) for a mean JONSWAP spectrum and $B = 0.2$

$$r = \frac{3\pi^3}{8}\frac{\rho_a}{\rho_w} B \frac{I_3}{I_4} = 0.365 \times 10^{-2} \text{ rad} \quad (46)$$

is in agreement with this result. Graber and Madsen (1982) have demonstrated that in deep water the advection coefficients D_{6j} differ in magnitude depending on the formulation, energy flux or wave momentum, used in the definition of the mean windsea direction. However, for practical applications in deep water, it was shown that either model formulation produces only small differences in the predicted wave parameters.

5. Migration of the spectral peak

It is generally agreed that in deep water the spectral peak of wind waves shifts towards lower frequencies as a consequence of the nonlinear energy transfer. Input from the wind occurs over the central region of the spectrum and wave-wave interaction processes rapidly redistribute the enhanced energy level towards lower and higher frequencies. In the high-frequency equilibrium range, the input and nonlinear transfer terms are balanced by white-capping dissipation processes.

As surface waves propagate into waters of finite depth, the low-frequency spectral components interact with the bottom. This interaction rapidly increases in strength until ultimately all spectral components are engulfed in water depths shallow enough for even the high-frequency tail to feel the bottom. The resulting bottom frictional dissipation can absorb either all or part of the energy transferred by wave–wave interactions. The effect is reflected in the behavior of the spectral peak by slowing down the rate of migration towards lower frequencies or even totally reversing the trend of the shift. Evidence supporting the importance of bottom friction was given by Bouws and Komen (1983) who found in their analysis of storm waves in the North Sea that bottom friction was considerably larger than the nonlinear transfer term.

As a starting point in describing the migration of the peak we examine the parametric equation for the parameter f_m to attempt to quantify the rate and the sense of the shift as a function of dimensionless depth and bottom roughness. Thus, for spatially homoge-

neous cases in an ocean of constant depth this equation simplifies to

$$\frac{\partial f_m}{\partial t} = S^1_{nl} + S^1_{bf} \tag{47}$$

where S^1_{nl} and S^1_{bf} are given by (34) and (38), respectively. Since S^1_{nl} is always negative, we normalize (47) by $-S^1_{nl}$ to preserve the sign of the dimensionless rate for the spectral peak shift, i.e.,

$$\frac{\partial f^*_m}{\partial t} \equiv \frac{-1}{S^1_{nl}} \frac{\partial f_m}{\partial t} = -\left(1 + \frac{S^1_{bf}}{S^1_{nl}}\right) = 73.4 \frac{f_w \Gamma I_1^{1/2}}{R} - 1 \tag{48}$$

for a mean JONSWAP spectrum ($\gamma = 3.3$, $\sigma_a = 0.07$, $\sigma_b = 0.09$) and $\alpha = 0.01$. Figure 2 shows the nondimensional migration of the spectral peak for different friction factors. Positive values indicate that bottom friction dominates and hence the trend of the peak frequency to shift towards higher frequencies. It is evident that bottom friction factors $f_w \leq 0.01$ would slow down the shift of the peak towards lower frequencies but not completely stop this trend in any water depth. However, for $f_w \geq 0.01$ bottom friction dominates the low-frequency energy balance, causing the peak to migrate towards higher frequencies over a wide range of water depths. It should be noted that there are two zero-crossing points which indicate that bottom friction and nonlinear transfer balance each other. The first turning point results when frictional attenuation grows as the waves move into shallower water depths. The second crossing point occurs because the scaling factor

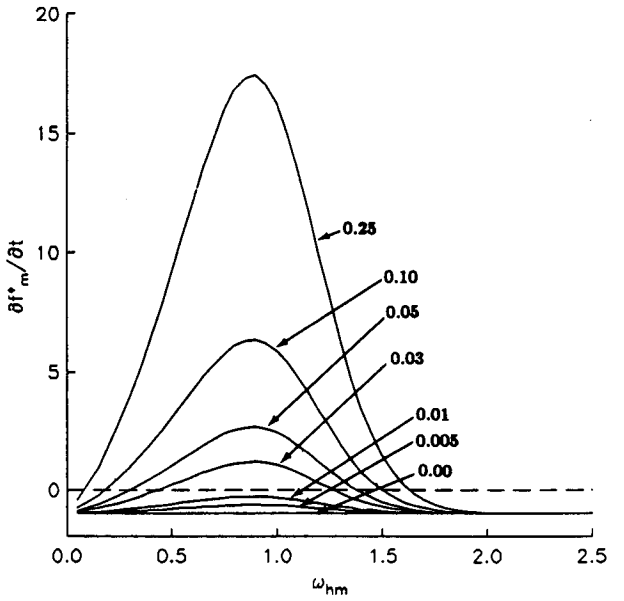

FIG. 2. Dimensionless rate of peak migration against dimensionless depth for different bottom friction factors.

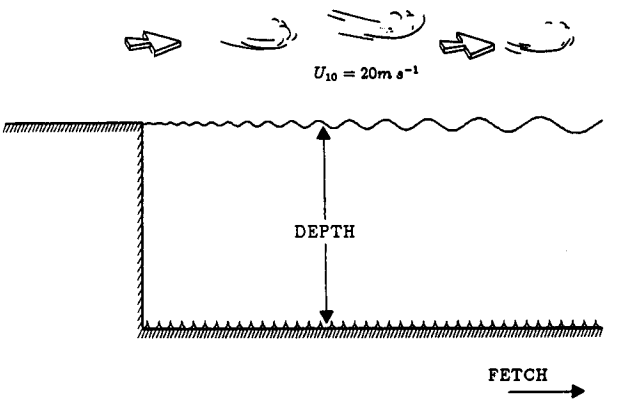

FIG. 3. Configuration of fetch-limited wave generation over flat but rough bottom in steady, homogeneous offshore winds.

R for the nonlinear transfer in finite depth increases very rapidly. As already mentioned, the simple scaling relation $R(\omega_{hm})$ is not applicable for $\omega_{hm} < 0.4$. Hence, the second cross-over point is an artifact of the parametrization of the nonlinear energy transfer in finite depth.

However, the location of the first turning point may be used to explore the existence of equilibrium spectra in shallow water. From the analysis of the Texel storm by Bouws and Komen (1983) we obtain $\omega_{hm} \approx 1.05$ and $f_w \approx 0.015$. From Fig. 2 these values suggest, at least qualitatively, that the storm spectrum was approximately in equilibrium. This fact seems to be confirmed from wave height measurements which remained at a constant level for approximately 12 hours (Fig. 1 in Bouws and Komen 1983).

6. Idealized test cases

Unfortunately there are no stretches on the continental shelf or in coastal embayments where the water depth is less than 50 m and remains constant for hundreds of kilometers. This fact prevents scientists from making measurements of simple wave generation cases to test and enhance our understanding of the physics of wave growth in depth-limited situations. In a similar way as done in the deep-water model intercomparison study SWAMP (1984) we can design idealized wind-wave generation cases to expose the model to influences caused by wave-bottom interactions. A similar exercise has been carried out in the SWIM (1985) study, where three operational shallow water wave models are intercompared. The motivation for this study is to investigate the role of realistic bottom friction estimates on the development of the spectrum in finite depth. We consider two hypothetical wave generation cases: 1) fetch-limited wave growth in an ocean of constant depth and 2) onshore propagation of a fully-developed deep-water windsea.

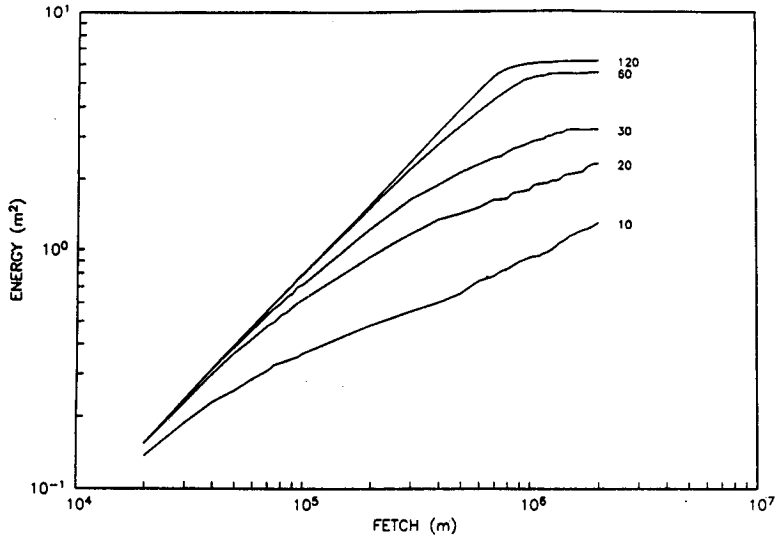

FIG. 4a. Growth curves of total energy E (m^2) against fetch X (m) as a function of friction factor f_w = 0.0 and depth (h = 10, 20, 30, 60, 120 m) for Case 1.

Case 1: Fetch-limited wave growth over a flat, rough bottom in steady, uniform 20 m s^{-1} offshore winds

The purpose of this test is to study wave development in the presence of a natural bottom along the fetch of a steady wind of 20 m s^{-1} for different water depths (see Fig. 3). Representative depths are chosen as: h = 10, 20, 30, 60, 120 m. The computations start at a fetch of 5 km and extend to 2000 km. The numerical simulations are conducted in two segments: (i) from 5 to 200 km at a spatial resolution of 5 km and a time step of 180 seconds, and (ii) from 50 to 2000 km at 50 km grid spacing and a time step of 900 seconds. Each run extends well beyond the time when stationary conditions are reached, i.e., for (i) 75 hours and for (ii) 200 hours. The initial conditions for all the model runs correspond to a JONSWAP spectrum at fetch 5 km, i.e., f_m = 0.329 Hz, α = 0.0253, γ = 3.3, σ_a = 0.07 and σ_b = 0.09. Corresponding to this input spectrum the waves are essentially deep-water waves for all water depths. However, for shallower water depths at a fetch equal to 50 km the waves are in some cases affected by the presence of the bottom. Therefore, time series of the predicted JONSWAP parameters at fetch 50 km from the short fetch simulations are used as boundary conditions for the long fetch runs. This approach ensures that the predicted wave conditions are independent of grid spacing for the overlap region (50 to 200

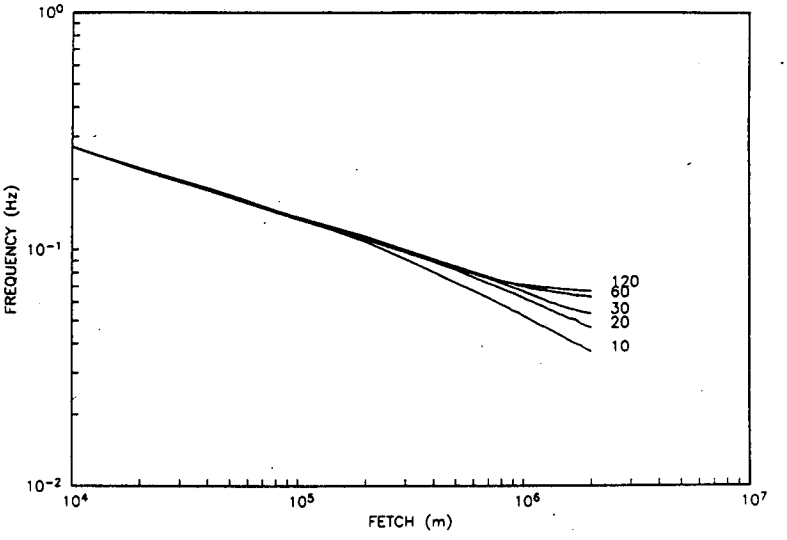

FIG. 4b. Plots of peak frequency f_m (Hz).

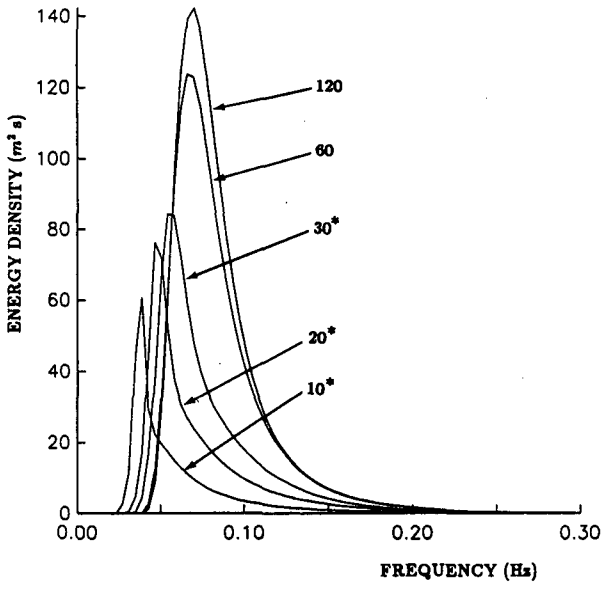

FIG. 4c. Wave energy spectra as a function of depth (m) at maximum fetch (2000 km) and duration (200 h). The asterisk indicates "equilibrium" not being attained.

km). As discussed in section 4c a single friction factor does not simulate accurately the fluid-sediment interaction illustrated in Fig. 1. However, to retain overall simplicity constant wave friction factors $f_w = 0.0, 0.005, 0.01, 0.03, 0.05$ and 0.1 were chosen in the computations. While the value $f_w = 0.0$ represents an idealized frictionless bed, the nonzero values may, with reference to Fig. 1, be thought of as representing flat immobile bed conditions (0.005 and 0.01), i.e., absolute *minimum* values, and *minimum* mobile bed friction (0.03, 0.05 and 0.1) for sediments ranging from silts to coarse sands. The results are displayed in terms of total energy and peak frequency as a function of fetch and the one-dimensional energy spectrum for maximum fetch and duration.

Figure 4 shows the results obtained for the idealized frictionless bottom case, $f_w = 0.0$. It is noticed in Fig. 4a that the growth curves for water depths 10 and 20 m have not leveled off as the maximum fetch is approached. This feature is also exhibited in Fig. 4b in that the peak frequencies are still decreasing as maximum fetch is approached. However, in Fig. 4b the curve for 30 m depth, in addition to those for 10 and 20 m, has not reached equilibrium. As discussed in section 4a this behavior is associated with the fact that the chosen wind speed, 20 m s^{-1}, exceeds the maximum phase velocity, $c_{max} = (gh)^{1/2}$, for water depths of 30 m and less. For larger depths than 30 m equilibrium is reached in the frictionless case. In fact, the growth curve for 120 m water depth is effectively the deep-water curves and identical to the HYPA curve in the SWAMP (1984) study. At 200 km fetch the finite-depth effect on the nonlinear transfer source terms becomes noticeable and stratifies the peak frequencies so that the peak frequency of the one-dimensional spectra at the maximum fetch, Fig. 4c, increases with increasing water depth.

For $f_w = 0.01$, friction is beginning to show its influence, as was anticipated from the discussion in Section 5 and the results shown in Fig. 2. Wave growth in shallower water is clearly suppressed which is indicated by the gradual leveling of the growth curves (Fig. 5a). For the lowest depth, growth has been reduced by as much as 50%. The frequency of the spectral peak

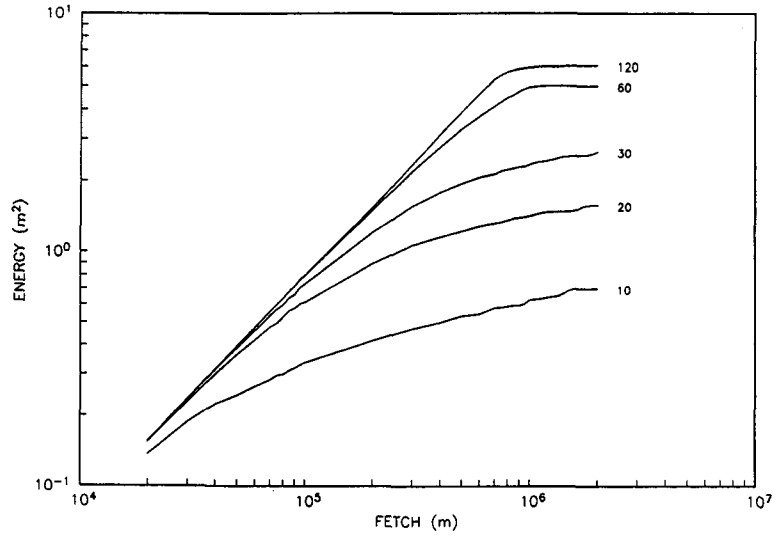

FIG. 5a. Growth curves of total energy E (m^2) against fetch X (m) as a function of friction factor $f_w = 0.01$ and depth (h = 10, 20, 30, 60, 120 m) for Case 1.

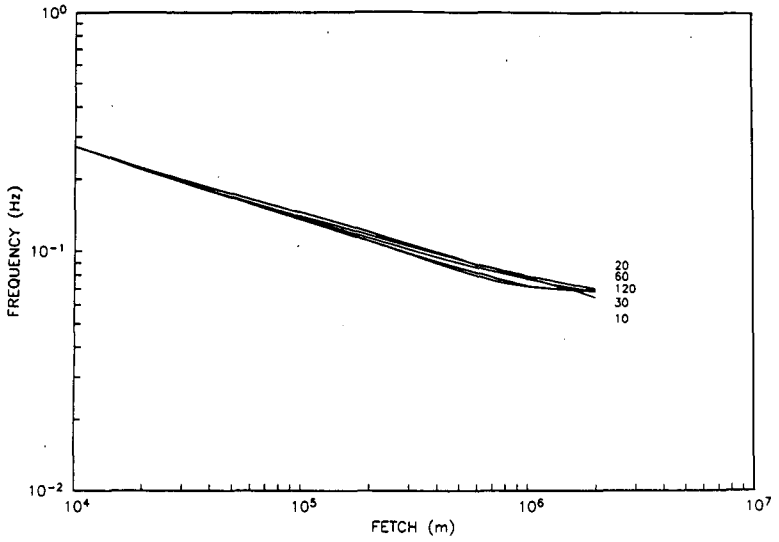

FIG. 5b. Plots of peak frequency f_m (Hz).

develops with fetch as in deep water and shows little sensitivity to the presence of a bottom (Fig. 5b). The spectral peak densities are considerably decreased, even for the 60 m spectrum (Fig. 5c). A closer look reveals that the peaks are located at almost the same frequency. This situation closely corresponds to the minimum bottom friction necessary to balance the positive low-frequency lobe of the nonlinear energy transfer.

Any additional drag felt by waves would lead to reversing the trend of a shift towards higher peak frequency with increasing depth. This is demonstrated in Fig. 6 which shows depth-limited wave growth when bottom friction, $f_w = 0.03$, dominates the spectral shape. After about 300 km the 20 and 30 m growth curves have attained a maximum which has significantly less total energy than any of the previous cases. For $h = 10$ m, total energy ceases to grow at 200 km (Fig. 6a). The influence of the bottom drag is now felt by waves in waters 120 m deep and less. These are typical depths found on the continental shelf along the east coast of North America and in the North Sea. The peak frequencies are stratified again, but now in order of decreasing depth (Fig. 6b). It is evident from this plot that the peak has migrated to significantly higher frequencies due to the enhanced bottom dissipation. Figure 6c shows the plot of spectra at infinite fetch and duration. Notice the drastically reduced energy densities for $h \leq 30$ m and the peak migration to the high frequency side. It is emphasized that the influence of bottom friction is quite pronounced for this case despite the value of $f_w = 0.03$ being representative of a minimum mobile flat bed friction for a silt-sized bottom sediment (cf. Fig. 1).

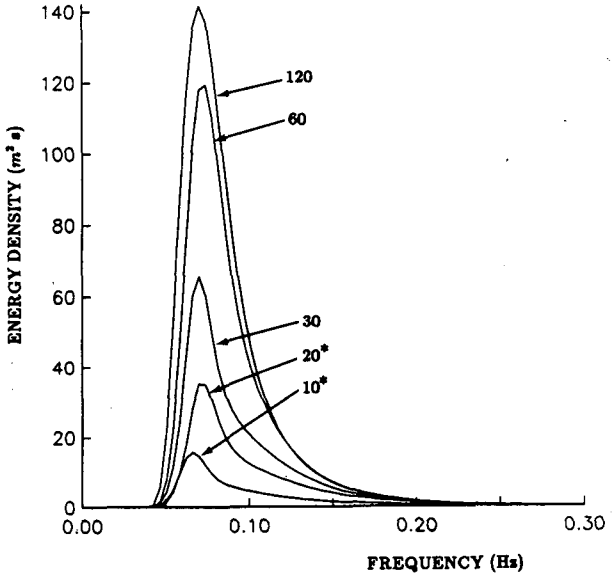

FIG. 5c. Wave energy spectra as a function of depth (m) at maximum fetch (2000 km) and duration (200 h). * indicates "equilibrium" not being attained.

A further increase in the friction factor, $f_w = 0.05$ and 0.1, results in strongly attenuated wave conditions. Wind-generated waves in 10 m water depths can barely retain the energy input by the wind since friction rapidly dissipates the available energy. Even for seas 60 m deep, the waves experience enough resistance to become dissipation limited. The peak frequencies are separated more which indicates that the influence of a natural, mobile bottom is felt by a windsea in shallow water for fetches less than 50 to 100 km. Additional trimming of the energy peaks and stratification towards higher frequencies become evident for all depths. However, the nature of the evolution is for the higher values of f_w, in principle, not different from that rep-

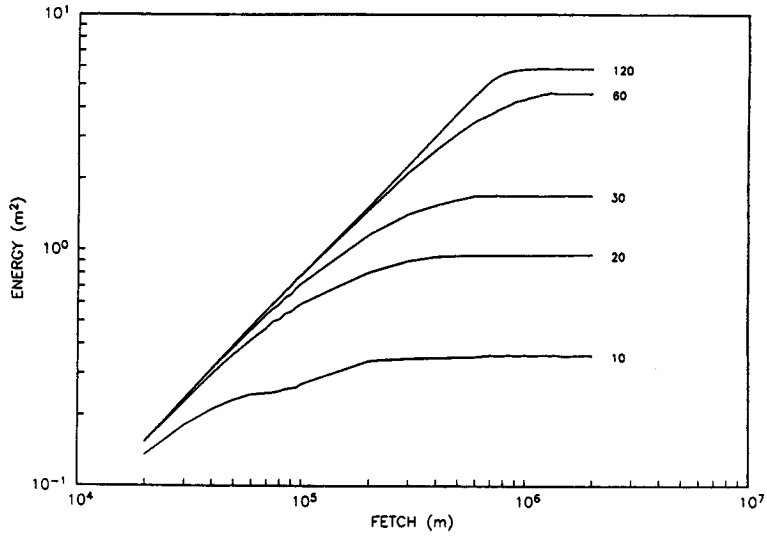

FIG. 6a. Growth curves of total energy E (m^2) against fetch X (m) as a function of friction factor $f_w = 0.03$ and depth (h = 10, 20, 30, 60, 120 m) for Case 1.

resented in Fig. 6. A summary of the limiting significant wave heights and peak frequencies corresponding to the maximum fetch are given in Table 2 for all values of f_w used in the computations.

Case 2: Wave propagation over a gently sloping, rough bottom at normal incidence under influence of a 20 m s^{-1} wind

The objective of this test is to understand how a deep-water Pierson–Moskowitz spectrum (fully developed windsea) is transformed by finite-depth effects when propagating into shallow seas up a gently sloping bottom (Fig. 7). Here we consider constant bottom slopes of 10^{-4} and 10^{-3}, typical for continental shelves and marginal seas. Since the angle of incidence is taken to be normal to the bottom contours, we investigate only the combined shoaling and bottom dissipation effect on wave evolution. As in the previous case, wave attenuation is studied for a range of friction factors. The runs were started from a flat sea with a constant wind blowing onshore at 20 m s^{-1} and were continued until the wave field reached stationary state, with a fully developed spectrum as the deep-water boundary condition. The depths at the offshore and inshore ends are 250 and 10 m. Only the result of the stationary solutions is presented.

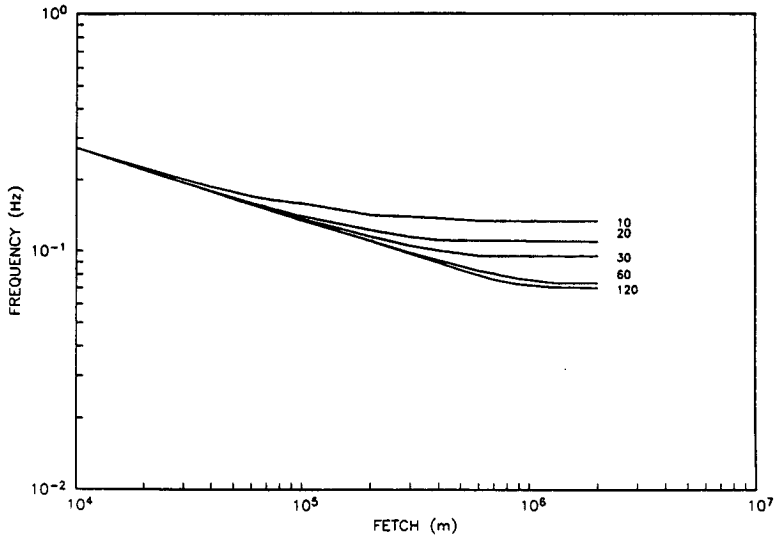

FIG. 6b. Plots of peak frequency f_m (Hz).

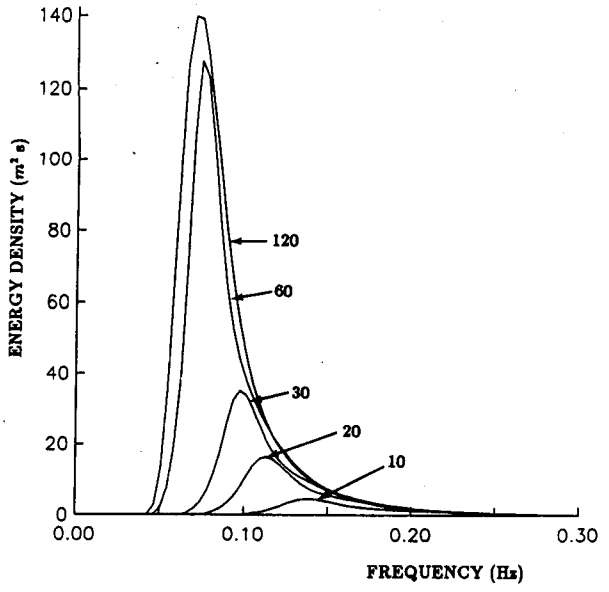

FIG. 6c. Wave energy spectra as a function of depth (m) at infinite fetch and duration.

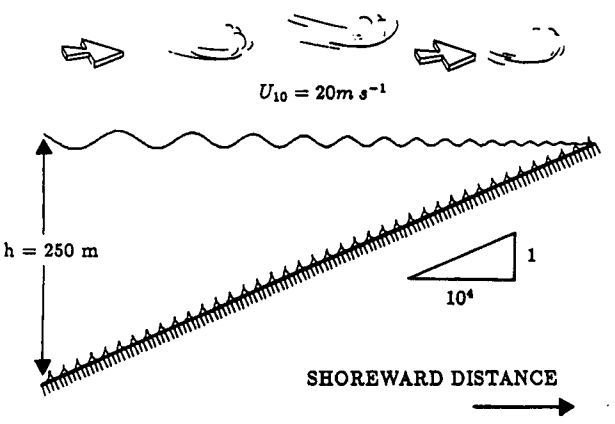

FIG. 7. Configuration of wave transformation over a gently sloping, rough bottom at normal incidence.

The variation of the wave field along the shelf slope of 10^{-4} is shown in Fig. 8 for the different friction factors characterizing the bottom roughness. Most noticeable is the dramatic reduction in energy as the waves propagate up the slope (Fig. 8a). While this decrease in the frictionless case ($f_w = 0.0$) is associated with the increased dissipation through wave breaking, represented by the Kitaigorodskii transformation factor, the additional effect of bottom frictional attenuation is clearly evident in water depths of less than 100 m becoming pronounced in depths less than about 50 m. The effect of bottom friction on peak frequency is demonstrated in Fig. 8b by the increase in peak frequency with increasing friction factor. The stationary energy spectra obtained for 10 m water depth, shown in Fig. 8c, clearly demonstrate how strongly shallow water wave climates depend on offshore bottom roughness (friction factor). The results shown in Fig. 8 are representative also for the variation along a 10^{-3} slope, when it is recognized that a steeper slope decreases the distance traveled by the waves and hence reduces frictional effects relative to those exhibited in Fig. 8.

To examine the nature of the stationary waves obtained in a given water depth as a function of bottom slope and friction, Tables 3 and 4 present significant wave heights and peak periods for different depths and friction factors for slopes of 10^{-4} and 10^{-3}, respectively. The results in those tables may be directly compared to the constant depth conditions reported in Table 2. When making this comparison it should be recalled that no equilibrium condition is reached for small depths and low friction factors. However, for relatively large friction factors and small depths (upper right hand corners of Tables 2, 3 and 4) the equilibrium wave heights decrease with decreasing slope while peak frequencies increase. This behavior represents the extent to which frictional effects have sufficient time to control the wave characteristics. In this respect it is interesting to note that the constant depth equilibrium wave characteristics are within 15% of the 10^{-4} slope results for the smaller water depths (less than 30 m) and larger

TABLE 2. Significant wave height $H_{1/3}$ (m) and peak frequency f_m (Hz) at maximum fetch and duration for Case 1. Asterisk values do not correspond to equilibrium conditions.

Depth (m)	f_w 0.0		0.005		0.01		0.03		0.05		0.10	
	$H_{1/3}$	f_m	$H_{1/3}$	f_m	$H_{1/3}$	f_m	$H_{1/3}$	f_m	$H_{1/3}$	f_m	$H_{1/3}$	f_m
10	4.58*	0.0370*	3.85*	0.0478*	3.34*	0.0641*	2.39	0.1340	2.13	0.1595	1.90	0.1812
20	6.10*	0.0469*	5.49*	0.0568*	5.01*	0.0697*	3.91	0.1096	3.56	0.1226	3.24	0.1337
30	7.18*	0.0537*	6.88*	0.0594*	6.51	0.0677	5.21	0.0955	4.78	0.1045	4.33	0.1138
60	9.42	0.0631	9.16	0.0666	8.94	0.0694	8.55	0.0735	8.12	0.0772	7.14	0.0856
120	9.95	0.0666	9.89	0.0687	9.84	0.0690	9.66	0.0700	9.55	0.0711	9.38	0.0728

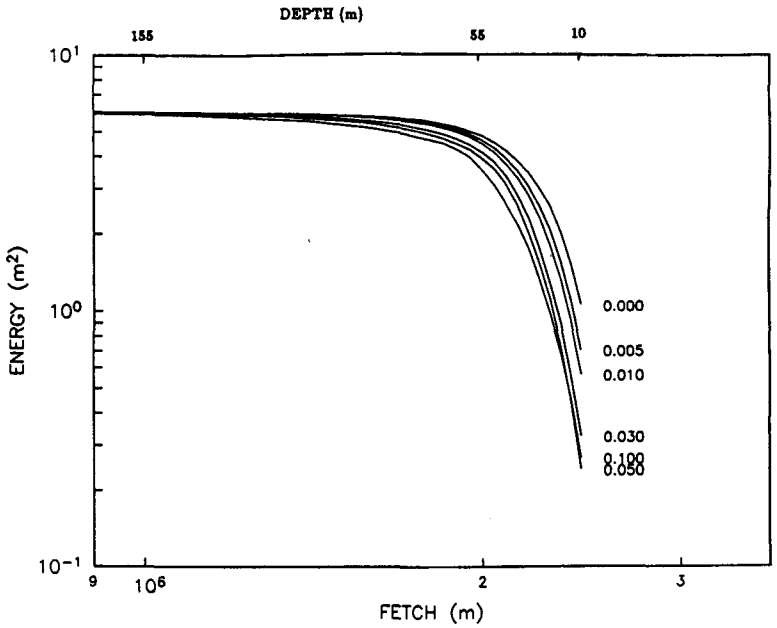

FIG. 8a. Stationary distribution of total energy E (m^2) along shoreward distance X (m) and as function of friction factors (f_w = 0.0, 0.005, 0.01, 0.03, 0.05, 0.1) for constant slope 10^{-4} starting in deep water at h = 250 m.

friction factors ($f_w \geq 0.03$). Thus, for a sufficiently gentle slope over a relative rough bottom the wave evolution may be thought of as frictionally dominated.

7. Conclusions

An alternative derivation for a parametric windsea model is described, which is governed by a transport equation for energy flux. The model is based on the premise that the inclusion of a mean wave direction calls for a vector quantity that describes a kinematic aspect of the wave field. The model is extended to incorporate finite-depth mechanisms such as shoaling, refraction and dissipation by bottom friction. The atmospheric input and nonlinear energy transfer terms are modified to account for finite-depth effects.

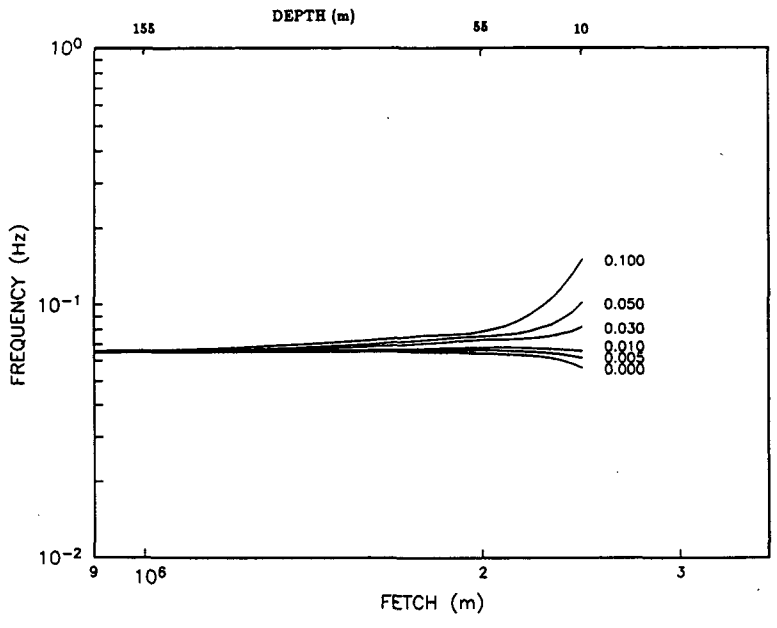

FIG. 8b. Plot of stationary distribution of peak frequency f_m (Hz) as function of friction factors for 10^{-4} slope.

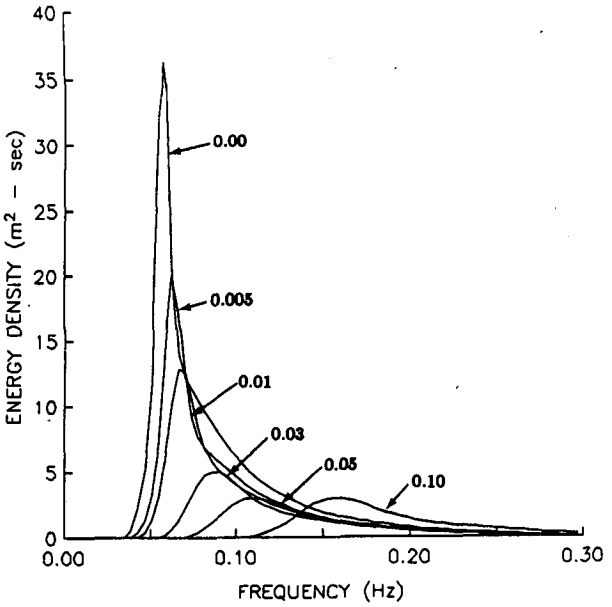

FIG. 8c. Plot of stationary wave energy spectra in limiting depth h = 10 m as function of friction factors for 10^{-4} slope.

From the transport equation for the peak frequency f_m we examine the possibility for the existence of an equilibrium spectrum in finite depth. From this balance equation we hypothesize that an equilibrium spectrum occurs when the nonlinear energy transfer across the peak is equal and opposite to the loss of energy caused by the waves interacting with a rough bottom. This condition results in a stationary location of the peak within the spectrum, which otherwise would move towards lower frequencies if nonlinear wave-wave interactions dominate the spectral dynamics or wander towards higher frequencies if the ocean bottom is sufficiently rough to cause a large loss in wave energy. It is encouraging that numerical simulations for various conditions of the bottom roughness yield reasonable limiting wave heights and peak frequencies for two idealized situations of wave growth and propagation. However, quantitative verification of our results awaits further wave measurements combined with the detailed simultaneous specification of the space-time structure of the bottom roughness.

We have tested the response of the model for diverse roughness conditions on a flat seabed under steady, homogeneous offshore winds in different water depths. The results are presented in terms of the evolution of total energy and peak frequency against fetch. The limiting values of significant wave height and peak frequency are summarized and clearly demonstrate the trend of decreasing energy and increasing peak frequency for rougher ocean bottom. The second test was designed to understand the transformation of a fully developed offshore spectrum propagating up a constant and rough slope in steady uniform onshore winds. This numerical simulation was used to examine the behavior of the wave spectrum with the additional process introduced by shoaling. The stationary solution of the transformed wave field shows the same general trend as in Case 1.

In view of the conservatively low choice of friction factors representing wave interaction with natural sediments, our results support the following conclusions: 1) bottom friction is an effective process attenuating wave energy for the space and time scales applicable to continental shelves; 2) the resistance felt by surface waves extends from the shallow depths of the coastal zone to the typical depths found on shelves and in marginal seas; 3) interactions of waves and rough bottom is a dissipative mechanism which plays an equally important role to that of nonlinear wave–wave interactions in the evolution of the wave spectrum in finite depth; 4) the net effect of these two processes controls the migration of the spectral peak; 5) the turning points (i.e., the nonlinear transfer balances bottom friction), are possible locations where equilibrium sea states may exist and occur when the direction of the spectral peak shift along the frequency axis is reversed; 6) shoaling, in general, reduces the strong influence of bottom friction on the spectral energy balance and tends to slow down the migration rate of the spectral peak.

The finite-depth wind-wave model formulation presented in this paper avoided the introduction of any "new" coefficients for which values must be obtained prior to application. In a forthcoming paper the model

TABLE 3. Significant wave height $H_{1/3}$ (m) and peak frequency f_m (Hz) at stationary conditions as a function of f_w and depth (h = 10, 20, 30, 60 and 120 m) for Case 2, 10^{-4} slope.

	f_w											
	0.0		0.005		0.01		0.03		0.05		0.10	
Depth (m)	$H_{1/3}$	f_m	$H_{1/3}$	f_m	$H_{1/3}$	f_m	$H_{1/3}$	f_m	$H_{1/3}$	f_m	$H_{1/3}$	f_m
10	4.12	0.0563	3.37	0.0617	3.01	0.0657	2.29	0.0820	1.97	0.1024	2.07	0.1512
20	5.67	0.0604	4.98	0.0638	4.59	0.0665	3.77	0.0772	3.40	0.0879	3.30	0.1173
30	6.89	0.0625	6.38	0.0651	6.05	0.0673	5.26	0.0745	4.92	0.0813	4.58	0.0977
60	8.94	0.0647	8.82	0.0663	8.71	0.0678	8.41	0.0725	8.25	0.0751	7.98	0.0773
120	9.71	0.0654	9.69	0.0656	9.67	0.0658	9.62	0.0667	9.58	0.0674	9.45	0.0692

TABLE 4. Significant wave height $H_{1/3}$ (m) and peak frequency f_m (Hz) at stationary conditions as a function of f_w and depth (h = 10, 20, 30, 60 and 120 m) for Case 2, 10^{-3} slope.

Depth (m)	f_w = 0.0		0.005		0.01		0.03		0.05		0.10	
	$H_{1/3}$	f_m	$H_{1/3}$	f_m	$H_{1/3}$	f_m	$H_{1/3}$	f_m	$H_{1/3}$	f_m	$H_{1/3}$	f_m
10	4.26	0.0629	3.98	0.0633	3.78	0.0638	3.31	0.0656	3.02	0.0675	2.56	0.0724
20	5.59	0.0634	5.42	0.0637	5.25	0.0641	4.83	0.0656	4.52	0.0671	4.01	0.0710
30	6.45	0.0637	6.36	0.0640	6.28	0.0643	5.97	0.0655	5.75	0.0668	5.28	0.0700
60	7.97	0.0648	7.95	0.0650	7.92	0.0651	7.82	0.0657	7.74	0.0664	7.53	0.0679
120	9.36	0.0656	9.35	0.0656	9.35	0.0656	9.33	0.0657	9.32	0.0658	9.27	0.0660

will be applied to an intense storm over the East Coast continental shelf.

Acknowledgments. The work reported here was carried out, while the first author was a student at the Massachusetts Institute of Technology, and received financial support from NOAA's Office of Sea Grant, U.S. Department of Commerce, under Grant NA 81AA-D-00069. The completion and final preparation of the research described in this paper was carried out at the Woods Hole Oceanographic Institution and the support of NOAA's Office of Sea Grant, U.S. Dept. of Commerce, under Grant NA86-AA-D-SG090, WHOI Sea Grant Project No. R/M-12 is gratefully acknowledged. The first author also wishes to thank Heinz Günther and Wolfgang Rosenthal from the GKSS Research Center for many helpful discussions. We thank Kenneth Borowski for the graphics.

APPENDIX A

Refraction and Group Velocity Divergence Terms

The evaluation of the R_i terms follows the basic method discussed by Günther et al. (1981). For the sake of brevity we present only the final steps leading up to the parametric expressions. After some lengthy algebraic manipulations one arrives at this compact formulation

$$R_i = -\frac{8}{3\pi}\hat{R}_i\left(\sin\theta_0\frac{\partial h}{\partial x} + \cos\theta_0\frac{\partial h}{\partial y}\right) \quad \text{for} \quad i = 1, \cdots, 5 \quad \text{(A1)}$$

where

$$\hat{R}_i = \phi_i'\left\{\frac{\omega}{2}\frac{\chi^2-1}{\chi}\left[\frac{2(1-\omega_{hm}^2)}{1+\omega_{hm}^2(\chi^2-1)}\right]E_J(f)\right\}$$

and the term in parentheses of (A1) represents the change in water depth parallel to the mean windsea direction. Evaluation of the operation ϕ_i' yields the following result:

$$\hat{R}_1 = 2\pi f_m^2 K\Delta_0 \quad \text{(A2)}$$

$$\hat{R}_2 = 2\pi\alpha f_m[I_5 + 0.722K\Delta_0] \quad \text{(A3)}$$

$$\hat{R}_3 = 2\pi\gamma f_m[\Delta_1 + 4.278K\Delta_0 - I_5] \quad \text{(A4)}$$

where

$$\Delta_0 = \frac{\chi^2-1}{\chi(1+\Omega)}\left[1 - 3\omega_{hm}^2 - \frac{4\omega_{hm}^2\chi^2(1-\omega_{hm}^2)}{(1+\Omega)^2}\right]$$

$$\Delta_1 = \frac{\chi^2-1}{\chi}\left(\frac{1-\omega_{hm}^2}{1+\Omega}\right)$$

$$\Omega \equiv \omega_{hm}^2(\chi^2-1)$$

$$I_5 = \frac{\omega_{hm}^{-2}}{0.65}\int_{1.35\omega_{hm}}^{2\omega_{hm}} \omega_h\frac{(\chi^2-1)}{\chi}\frac{(1-\omega_h^2)}{1+\omega_h^2(\chi^2-1)}\,d\omega_h.$$

In deep water $\chi \to 1$ and all the $\hat{R}_i$ terms vanish identically. In shallow water, i.e., $\omega_{hm} < 0.4$, with $\chi \to \omega_h^{-1}$, the integrand takes on the form $\sim(1-\omega_h^2)^2/(2-\omega_h^2)$ and may be evaluated analytically.

The derivation for an appropriate expression R_6 must necessarily reveal a dependence on the depth gradient perpendicular to the mean windsea direction. From the definition of ϕ_6' in (19) the subsequent parametric relation emerges expressing the response of the windsea spectrum to a variable bottom topography

$$R_6 = -\frac{3}{32}\pi^2 f_m\omega_{hm}^{-1}\frac{J_1}{J_2}\left(\cos\theta_0\frac{\partial h}{\partial x} - \sin\theta_0\frac{\partial h}{\partial y}\right) \quad \text{(A5)}$$

where

$$J_1 = \omega_{hm}^4\int_0^\infty \omega_h^{-5}\frac{\chi^2-1}{\chi}\left[3 + \frac{2(1-\omega_h^2)}{1+\omega_h^2(\chi^2-1)}\right] \times \psi\left(\frac{\omega_h}{\omega_{hm}}, \gamma, \sigma\right)d\omega_h \quad \text{(A6)}$$

and J_2 is given by (B7).

APPENDIX B

Depth Dependent Advection Terms

The determination of the D_{ij} in Table 1 is straightforward by applying the appropriate mapping functionals:

$$D_{ij} = \phi_i'\left\{c_g(f, h)\frac{\partial\mathcal{E}}{\partial a_j}\right\} \quad \text{for} \quad i, j = 1, \cdots, 5. \quad \text{(B1)}$$

From the evaluation of operation (B1) if follows that

$$\xi_0 = K\left[1 - 4\frac{\omega_{hm}^2(\chi^2-1)(1-\omega_{hm}^2)}{(1+\omega_{hm}^2(\chi^2-1))^2}\right]. \quad \text{(B2)}$$

Similarly, expressions for ξ_1 and ξ_2 can be calculated

$$\xi_1 = 0.722 - \frac{5\omega_{hm}^4\chi}{0.65[1+\omega_{hm}^2(\chi^2-1)]} \times \int_{1.35\omega_{hm}}^{2\omega_{hm}} \frac{1+\omega_h^2(\chi^2-1)}{\omega_h^5\chi}\, d\omega_h \quad \text{(B3)}$$

and

$$\xi_2 = \frac{\chi}{0.65[1+\omega_{hm}^2(\chi^2-1)]} \times \int_{1.35\omega_{hm}}^{2\omega_{hm}} \frac{1+\omega_h^2(\chi^2-1)}{\omega_h\chi}\, d\omega_h. \quad \text{(B4)}$$

The propagation terms D_{i6} are given by

$$D_{i6} = \alpha D_{i2} \quad \text{for} \quad i = 1, \cdots, 5. \quad \text{(B5)}$$

The group velocity c_{gm} corresponds to the velocity at peak frequency, f_m, in depth, h,

$$c_{gm} = \frac{g}{4\pi f_m}\chi^{-1}[1+\omega_{hm}^2(\chi^2-1)]. \quad \text{(B6)}$$

For the directional parameter $a_6 = \theta_0$, the advection terms are calculated from the operation ϕ_6' applied to the energy flux vector $\mathcal{E}(f, \theta, h)$. The nondimensional integrals depending only on the spectral shape and water depth are

$$J_2 = \omega_{hm}^5 \int_0^\infty \omega_h{}^{-6}\chi^{-3}\psi\left(\frac{\omega_h}{\omega_{hm}}, \gamma, \sigma\right) d\omega_h \quad \text{(B7)}$$

$$J_3 = \omega_{hm}^6 \int_0^\infty \omega_h{}^{-7}\frac{1+\omega_h^2(\chi^2-1)}{\chi^4} \times \psi\left(\frac{\omega_h}{\omega_{hm}}, \gamma, \sigma\right) d\omega_h. \quad \text{(B8)}$$

REFERENCES

Barnett, T. P., C. H. Holland, Jr. and P. Yager, 1969: A general technique for wind wave prediction, with application to the South China Sea. Final Report, U.S. Naval Oceanographic Office, 31 pp.

Bouws, E., and G. J. Komen, 1983: On the balance between growth and dissipation in an extreme depth-limited wind-sea in the southern North Sea. *J. Phys. Oceanogr.*, **13**, 1653–1658.

——, H. Günther, W. Rosenthal and C. L. Vincent, 1985: Similarity of the wind wave spectrum in finite depth water, 1. Spectral form. *J. Geophys. Res.*, **90**(C1), 975–986.

——, ——, —— and ——, 1987: Similarity of the wind wave spectrum in finite depth water, 2. Statistical relations between shape and growth stage parameters. *Dtsch. Hydrogr. Z.*, **40**, 1–24.

Cavaleri, L., and P. M. Rizzoli, 1978: A wind waves prediction model in the Adriatic Sea. *Turbulent Fluxes through the Sea Surface—Wave Dynamics and Prediction.* A. Favre and K. Hasselmann, Eds., Plenum Press, 629–644.

Collins, J. I., 1972: Prediction of shallow-water spectra. *J. Geophys. Res.*, 77(15), 2693–2707.

Donelan, M. A., 1977: A simple numerical model for wave and wind stress prediction. Unpublished manuscript. National Water Research Institute, Burlington, Ontario, 28 pp.

——, 1980: Similarity theory applied to the forecasting of heights, periods, and directions. *Proc. of the Canadian Coastal Conf.*, National Research Council, Ottawa, Ontario, 47–61.

Golding, B. W., 1978: A depth dependent wave model for operational forecasting. *Turbulent Fluxes through the Sea Surface—Wave Dynamics and Prediction.* A. Favre and K. Hasselmann, Eds., Plenum Press, 593–606.

——, 1983: A wave prediction system for real time sea state forecasting. *Quart. J. Roy. Meteor. Soc.*, **109**, 393–416.

Graber, H. C., 1984: A parametric wind-wave model for arbitrary water depths. Ph.D. dissertation, Massachusetts Institute of Technology, 310 pp.

——, and O. S. Madsen, 1982: The directional relaxation of a windsea spectrum using an energy flux approach. *Trans. Amer. Geophys. Union*, **65**(45), 970.

——, and ——, 1985: A parametric wind wave model for arbitrary water depths. *THE OCEAN SURFACE: Wave Breaking, Turbulent Mixing and Radio Probing.* Y. Toba and H. Mitsuyasu, Eds., D. Reidel, 193–199.

Grant, W. D., 1977: Bottom friction under waves in the presence of a weak current: Its relationship to sediment transport. Ph.D. dissertation, Massachusetts Institute of Technology, 275 pp.

——, and O. S. Madsen, 1979: Combined wave and current interaction with a rough bottom. *J. Geophys. Res.*, **84**(C4), 1797–1808.

——, and ——, 1982: Moveable bed roughness in unsteady oscillatory flow. *J. Geophys. Res.*, **87**(C1), 469–481.

——, and ——, 1986: The continental shelf bottom boundary layer. *Annual Review Fluid Mechanics*, **18**, 265–305.

Günther, H., and W. Rosenthal, 1983a: Self similarity of surface wave spectra in water of finite depth. *Sixth Australian Conf. on Coast. and Ocean Eng.*, 264–272.

——, and ——, 1983b: Shallow water surface wave model based on the TEXEL-MARSEN-ARSLOE (TMA) wave spectrum. Paper presented at *20th Congess, Int. Assoc. Hydraulic Res.*, Moscow, USSR.

——, ——, T. J. Weare, B. A. Worthington, K. Hasselmann and J. A. Ewing, 1979: A hybrid parametrical wave prediction model. *J. Geophys. Res.*, **84**(C9), 5727–5738.

——, —— and M. Dunckel, 1981: The response of surface gravity waves to changing wind direction. *J. Phys. Oceanogr.*, **11**, 718–728.

Hasselmann, D. E., M. Dunckel and J. A. Ewing, 1980: Directional wave spectra observed during JONSWAP 1973. *J. Phys. Oceanogr.*, **10**, 1264–1280.

Hasselmann, K., 1960: Grundgleichungen der Seegangsvoraussage. *Schiffstechnik*, **7**, 191–195.

——, 1974: On the spectral dissipation of ocean waves due to white capping. *Bound. Layer Meteor.*, **6**, 107–127.

——, and J. I. Collins, 1968: Spectral dissipation of finite-depth gravity waves due to turbulent bottom friction. *J. Mar. Res.*, **26**, 1–12.

——, T. P. Barnett, E. Bouws, H. Carlson, D. E. Cartwright, K. Enke, J. A. Ewing, H. Gienapp, D. E. Hasselmann, P. Krusemann, A. Meerburg, P. Müller, D. J. Olbers, K. Richter, W. Sell and H. Walden, 1973: Measurements of wind-wave growth and swell decay during the Joint North Sea Wave Project *(JONSWAP)*, *Dtsch. Hydrogr. Z.*, **A12**, 95 pp.

——, D. B. Ross, P. Müller and W. Sell, 1976: A parametric wave prediction model. *J. Phys. Oceanogr.*, **6**, 200–228.

Hasselmann, S., and K. Hasselmann, 1981: A symmetrical method of computing the nonlinear transfer in a gravity wave spectrum. *Hamburger Geophys. Einzelschriften*, Reihe A: Wissenschaftliche Abhandl., Heft 52.

——, and ——, 1985: Computations and parameterizations of the nonlinear energy transfer in a gravity wave spectrum. Part I: A

new method for efficient computations of the exact nonlinear transfer. *J. Phys. Oceanogr.*, **15**, 1369–1377.

Herterich, K., and K. Hasselmann, 1980: A similarity relation for the nonlinear energy transfer in a finite-depth gravity-wave spectrum. *J. Fluid Mech.*, **97**, 215–224.

Janssen, P. A. E. M., and W. J. P. de Voogt, 1985: On the effect of bottom friction on wind sea. *THE OCEAN SURFACE: Wave Breaking, Turbulent Mixing and Radio Probing.* Y. Toba and H. Mitsuyasu, Eds., D. Reidel, 185–192.

——, G. J. Komen and W. J. P. de Voogt, 1984: An operational coupled hybrid wave prediction model. *J. Geophys. Res.*, **89**(C3), 3635–3654.

Jonsson, I. G., 1966: Wave boundary layers and friction factors. *Proc. 10th Conf. Coastal Engineering*, **1**, 127–148.

Kajiura, K., 1964: On the bottom friction in an oscillatory current. *Bull. Earthquake Res. Inst.*, **42**, 147–174.

——, 1968: A model of the bottom boundary layer in water waves. *Bull. Earthquake Res. Inst.*, **46**, 75–123.

Kitaigorodskii, S. A., V. P. Krasitskii and M. M. Zaslavskii, 1975: On Phillips' theory of equilibrium range in the spectra of wind-generated gravity waves. *J. Phys. Oceanogr.*, **5**, 410–420.

Komen, G. J., S. Hasselmann and K. Hasselmann, 1984: On the existence of a fully developed wind-sea spectrum. *J. Phys. Oceanogr.*, **14**, 1271–1285.

McCowan, J., 1894: On the highest wave of permanent form. *Phil. Mag.*, Ser. 5, **38**, 351–358.

Madsen, O. S., and W. D. Grant, 1976: Sediment transport in the coastal environment. Tech. Rep. 209, R. M. Parsons Laboratory, Massachusetts Institute of Technology, 105 pp.

——, Y.-K. Poon, and H. C. Graber, 1988: Spectral wave attenuation by bottom friction. *Proc. 21st Int. Coastal Eng. Conf.*, ASCE. In press.

Miles, J. W., 1957: On the generation of surface waves by shear flows. *J. Fluid Mech.*, **3**, 185–204.

Phillips, O. M., 1957: On the generation of waves by turbulent wind. *J. Fluid Mech.*, **2**, 417–445.

Pierson, W. J., and L. Moskowitz, 1964: A proposed spectral form for fully developed wind seas based on the similarity theory of S. A. Kitaigorodskii. *J. Geophys. Res.*, **69**(24), 5181–5190.

Schwab, D. J., J. R. Bennett, P. C. Liu and M. A. Donelan, 1984: Application of a simple numerical wave prediction model to Lake Erie. *J. Geophys. Res.*, **89**(C3), 3586–3592.

Shemdin, O. H., S. V. Hsiao, H. E. Carlson, K. Hasselmann and K. Schulze, 1980: Mechanisms of wave transformation in finite depth water. *J. Geophys. Res.*, **85**(C9), 5012–5018.

Snyder, R. L., F. W. Dobson, J. A. Elliott and R. B. Long, 1981: Array measurements of atmospheric pressure fluctuations above surface gravity waves. *J. Fluid Mech.*, **102**, 1–59.

SWAMP Group, 1984: *OCEAN WAVE MODELING, I. The Sea Wave Modeling Project (SWAMP): Principal results and conclusions.*, Plenum Press, 256 pp.

SWIM Group, 1985: A shallow water intercomparison of three numerical wave prediction models. *Quart. J. Roy. Meteor. Soc.*, **111**, 1087–1112.

Trowbridge, J., and O. S. Madsen, 1984: Turbulent wave boundary layers 1. Model formulation and first-order solution. *J. Geophys. Res.*, **89**(C5), 7989–7997.